Solar Cells Hot Paper

DOI: 10.1002/anie.201402371

Constructing 3D Branched Nanowire Coated Macroporous Metal Oxide Electrodes with Homogeneous or Heterogeneous Compositions for Efficient Solar Cells**

*Wu-Qiang Wu, Yang-Fan Xu, Hua-Shang Rao, Hao-Lin Feng, Cheng-Yong Su, and Dai-Bin Kuang**

Abstract: *Light-harvesting and charge collection have attracted increasing attention in the domain of photovoltaic cells, and can be facilitated dramatically by appropriate design of a photonic nanostructure. However, the applicability of current light-harvesting photoanode materials with single component and/or morphology (such as, particles, spheres, wires, sheets) is still limited by drawbacks such as insufficient electron–hole separation and/or light-trapping. Herein, we introduce a universal method to prepare hierarchical assembly of macroporous material–nanowire coated homogenous or heterogeneous metal oxide composite electrodes (TiO_2–TiO_2, SnO_2–TiO_2, and Zn_2SnO_4–TiO_2; homogenous refers to a material in which the nanowire and the macroporous material have the same composition, i.e. both are TiO_2. Heterogeneous refers to a material in which the nanowires and the macroporous material have different compositions). The dye-sensitized solar cell based on a TiO_2-macroporous material–TiO_2-nanowire homogenous composition electrode shows an impressive conversion efficiency of 9.51%, which is much higher than that of pure macroporous material-based photoelectrodes to date.*

In recent years, a great deal of scientific and technical interest has been placed in hierarchical porous semiconducting metal oxide based materials, which have shown great potential in catalysis, energy conversion and storage, water splitting, or optoelectronics.[1] Porous materials with hollow structures have shown promising properties in processes involving interface- and transport-related dynamics. For specific applications, such as in solar cells, reinforced light-harvesting and charge-collection efficiency were obtained as a result of the prominent role played by the hollow structure in confining the incident light within the electrode by the Mie scattering mechanism, promoting electron transport and improving electrolyte penetration.[2]

The majority of reports on the hierarchical porous metal oxides have focused on the 2D hollow structure enclosed by single-crystalline nanoparticles,[3] or which combine large pores with walls containing small ones.[4] However, the dye-sensitized solar cells (DSSCs) based on purely macroporous photoelectrodes gave unsatisfactory photovoltaic performance because of their low surface area for poor dye loading.[3a–e,5]

To increase the dye loading, nanoparticle-filled macroporous materials have been found to improve the photovoltaic performance significantly.[4c] It is well established that 1D nanostructures, such as nanorods or nanowires, exhibit fast electron transportation and slow electron recombination, which contribute to the higher photocurrent density, voltage as well as power conversion efficiency.[6] Hence, a photoelectrode with a nanowire-coated macroporous material hybrid structure which combines the advantages of macroporous structure and nanowire may potentially improve the efficiency greatly. The key idea for these new forms of photoanode materials is to couple the nanowires with a hierarchical porous metal oxide backbone to achieve enhanced light scattering over greater length scales, high photosensitizer loading, and larger contact interface areas with the electrolyte. Recent 3D hierarchically ordered TiO_2 inverse-opal ZnO nanowire hybrid nanostructure showed a higher photocurrent than the TiO_2 inverse opal in quantum dot (QD) photoelectrochemical cells.[7] However, the ZnO may form the Zn^{2+}-dye complex which influences the photovoltaic performance of DSSC. In contrast, it is established that TiO_2 has a high isoelectric point that facilitates the adsorption of dye molecules with acidic carboxyl groups allowing ultra-fast photoelectron injection rates from excited dye, making it the most efficient metal oxide photoelectrode.[8] To our knowledge, reports concerning the facile solution growth of anatase TiO_2 nanowire branched networks on homogeneous pristine hollow TiO_2 scaffolds are scarce, as are those of its growth on other heterogeneous hollow metal oxides scaffolds.

Herein, typical metal oxide (i.e. TiO_2, SnO_2, Zn_2SnO_4) macroporous structures are used as the host template for the facile solution growth of anatase TiO_2 nanowires. Accordingly, we demonstrate three novel hierarchical macroporous oxide–TiO_2 nanowire hybrid nano-architectures consisting of, namely, rambutan-like TiO_2–TiO_2, sunflower-like SnO_2–TiO_2,

[*] W. Q. Wu, Y. F. Xu, H. S. Rao, H. L. Feng, Prof. Dr. C. Y. Su, Prof. Dr. D. B. Kuang
MOE Key Laboratory of Bioinorganic and Synthetic Chemistry, State Key Laboratory of Optoelectronic Materials and Technologies, Lehn Institute of Functional Materials, School of Chemistry and Chemical Engineering, Sun Yat-sen University
Guangzhou 510275 (P.R. China)
E-mail: kuangdb@mail.sysu.edu.cn

[**] We acknowledge financial support from the National Natural Science Foundation of China (U0934003, J1103305), the Program for New Century Excellent Talents in University (NCET-11-0533), the Fundamental Research Funds for the Central Universities, and the NSF of Guangdong Province (S2013030013474).

Supporting information for this article is available on the WWW under http://dx.doi.org/10.1002/anie.201402371.

and nest-like Zn_2SnO_4–TiO_2. Most importantly, this general method offers the possibility of realizing size-tunable preparation of metal oxide porous frameworks by a straightforward templating strategy while allowing well-crystallized anatase TiO_2 nanowire branches to germinate inside and outside the homogeneous or heterogeneous hollow material scaffolds using a simple solution process.

The overall fabrication method is based on the size-tunable preparation of macroporous host scaffolds by using monodisperse polystyrene (PS) spheres as sacrificial templates, and then extended to allow the facile solution growth of anatase TiO_2 nanowire branches to fill the macropores and the interstitial voids between spheres (Figure 1). A metal oxide (i.e., TiO_2 or SnO_2) thin blocking layer (ca. 100 nm) was pre-coated on F-doped SnO_2 conductive glass (FTO) to retard interfacial recombination between electrons in the highly conducting FTO and the I_3^- oxidized electrolyte.[9] The appropriate surface modification of FTO plays a vital role in reducing the recombination at the FTO/metal oxide interface and the grain boundaries of FTO.[10] The PS spheres were densely enclosed within metal oxide nanoparticles (MONPs) in a highly efficient and reproducible fashion by sol–gel refluxing or hydrothermal method using alternating metallic precursors. In the first stage, a uniform dispersion of metal oxide coated PS spheres (PS@MONPs) in ethanol solution was dip-coated on a blocking layer-coated FTO glass to give a large-area highly uniform film (Figure 1a). In the second step, the dried films underwent a burn-out process for decomposing the PS spheres which led to the formation of a highly crystalline macroporous metal oxide (MPMO) scaffold composed of nanoparticles (NPs; Figure 1b) that was well-connected to the underlying FTO glass front electrode. In contrast to the conventional periodic macroscopic structures that were fabricated by infiltration of nanoparticles onto self-assembled PS sphere scaffolds,[4c,d] the current macroporous scaffold exhibits imperfect periodicity and loose packing of hollows which enables filling of the guest TiO_2 nanowires in all three spatial dimensions later on. As shown in Figure S1 (X-ray diffraction (XRD), Supporting Information), macroporous materials with the cubic structure of Zn_2SnO_4, the cassiterite crystal structure of SnO_2, and anatase crystal structure of TiO_2 were obtained.

Figure 1c shows the formation of an intriguing 3D TiO_2 branched hierarchical macroporous metal oxide (3D TiO_2 branched MPMO) hybrid structure formed through the subsequent solution growth of anatase TiO_2 nanowires, in which multiple TiO_2 nanowires can randomly align and uniformly cover the entire pore surface of the macroporous scaffolds.

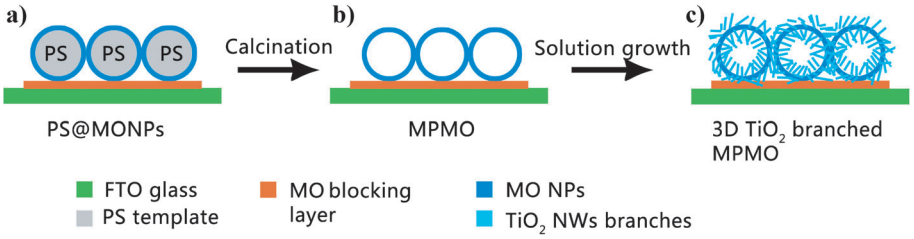

Figure 1. Procedure used to fabricate the 3D TiO_2 branched nanowire coated macroporous metal oxides. See text for details.

Figure 2a and b shows the top-view FE (field emission) SEM images of the macroporous TiO_2 (MP-TiO_2) hollow structures obtained by colloidal template-assisted method. The diameter of the hollow TiO_2 spheres is slightly less than that of original PS spheres (from 560 nm to 480 nm) and the sphere wall is formed from 10 nm nanoparticles. Special attention should be given to the "burst holes" which were probably produced as a result of PS decomposition during the high temperature calcination.[3a] The open holes, we believe, could allow easy penetration of dyes and electrolytes into the inner space of the hollow structures. Also, the accessible inner and outer surfaces of the hollow spheres are beneficial to enhance dye adsorption. For the fabrication of TiO_2 macroporous material–nanowire hybrid structure (MP-TiO_2-TNW), the macroporous TiO_2 films were impregnated with a surfactant-free precursor solution containing titanium potassium oxalate, water, and diethylene glycol

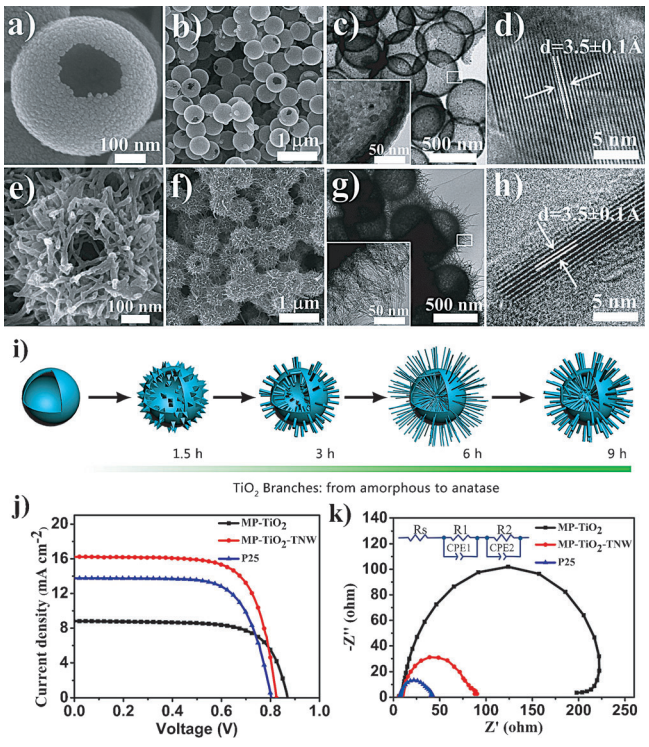

Figure 2. a,b) Top-view FE-SEM images of MP-TiO_2. c,d) TEM and HRTEM images of MP-TiO_2. e,f) Top-view FE-SEM images of MP-TiO_2-TNW. g,h) TEM and HRTEM images of MP-TiO_2-TNW. The insets of (c) and (g) show the magnified view of the marked white square area. i) Schematic illustration of growth mechanism for 3D TiO_2 branched hierarchical macroporous TiO_2. j) *J*–*V* curves and k) EIS spectra of MP-TiO_2, MP-TiO_2-TNW, and P25 based cells.

(DEG) and then treated hydrothermally. By adjusting the water/DEG volume ratio, hierarchical macroporous TiO_2 covered with different TiO_2 nano-branches were synthesized. Specifically, TiO_2 nano-branches evolved from 1D long thin nanowires to 0D nanoparticles (nanowires-nanorods-nanosheets-nanoparticles) along with decreasing DEG concentration (Figure S2), and in this case, DEG was employed as a capping agent to hinder the hydrolysis of titanium potassium oxalate and aids in directional growth of TiO_2 nanobranches.[11] Subsequently, the TiO_2 branched-nanowire-coated hierarchical macroporous TiO_2 hybrid structure prepared at a water/DEG volume ratio of 2.5:17.5 was selected as the most appropriate and promising candidates for DSSCs (seen Table S1). Figure 2e,f clearly show the 3D branched hierarchical hollow structure as well as the disorder packing inherited from the parental macroporous TiO_2 scaffolds. Note that multiple TiO_2 nanowires with tiny diameters and long lengths germinated on both sides (inner and outer) of each macroporous scaffold and homogeneously covered almost the entire pore throughout the whole film to form the rambutan-like TiO_2 nanostructures. The thickness of the hierarchical TiO_2 macroporous material–TiO_2 nanowire film is determined by the thickness of the parental TiO_2 macroporous scaffold (Figure S2). Subsequently, attempts to increase film thickness from 8 μm to 14 μm are successful by increasing the amount of dispersion, whereas further increase of the dispersion amount will result in the films cracking and peeling off the substrates. TEM images reveal that the hierarchical macroporous TiO_2 obtained is composed of crystalline anatase with crystal size of approximately 10 nm in the walls (Figure 2c and d). Visible in Figure 2g is the densely grown TiO_2 nanowires of approximately 3–5 nm in diameter and 150–200 nm in length within each macropore. The high magnification TEM image (Figure 2h) shows the nanowires are of high crystallinity with an interplane spacing of 3.5 ± 0.1 Å that closely matches the d-spacing of the (101) plane in anatase TiO_2.

Time-dependent experiments were carried out to shed light on the growth process of such intriguing 3D TiO_2 branched hollow structure. The samples prepared at different time intervals (1.5 h, 3 h, 6 h, 9 h) were characterized by SEM, TEM, and XRD, as shown in Figure S3 and Figure S4. The XRD patterns (Figure S3j) reveals that the nanowire branches were indexed as pure anatase TiO_2 (JCPDS No. 21-1271) with evidence of (101) and (200) preferred orientations and that a higher degree of crystallinity can be achieved with increasing reaction time. Based on the results from Figure S3 and S4, a diagram of the most plausible growth mechanism is shown in Figure 2i. In this process, the hierarchical macroporous TiO_2 spheres serve as the scaffolds, and the subsequent growth of TiO_2 nanowires branches experienced a self-template procedure. At the initial stage (1.5 h), a high concentration of DEG hinders the hydrolysis and facilitates the formation of thorn-like amorphous TiO_2 nanocrystals preferably on the surface of MP-TiO_2, and the average diameter and length of nanocrystal are 8–10 nm and 10–20 nm, respectively. When the reaction time was prolonged to 3 h, the amorphous nanocrystals were gradually crystallized and acted as cores to lead to the continuous growth of the crystallized nanowires. In this stage, some of the amorphous nanocrystals split into thinner nanowires of 5–8 nm in diameter and 40–60 nm in length. Interestingly, additional growth of TiO_2 nanowires can be observed on both the inner and outer wall of MP-TiO_2. As the reaction proceeded (6 h), the nanowires continuously grew in length (150–200 nm) with decreased diameter (3–5 nm) and the MP-TiO_2 was covered with interlaced and interconnected slender anatase TiO_2 nanowires. Strikingly, when the reaction was finally carried out for 9 h, even though more densely TiO_2 nanowires can be observed, the continuous growth of well-crystallized anatase nanowires occurred at the expense of a portion of the foregoing nanowires with poor stability, and thus resulting in the nanowires with larger diameter (5–8 nm) and shorter length (100–150 nm), which was mainly driven by the minimization of the system free energy during the hydrothermal process. Hence, the length of anatase TiO_2 nanowire can be conveniently controlled by adjusting the reaction time. Six hours growth of TiO_2 branches results in the formation of the longest and thinnest TiO_2 nanowires within the macropore scaffolds which provides an enhanced surface area for dye adsorption and facilitates the light-scattering. Interestingly the shape of 3D branched hierarchical macroporous TiO_2 somewhat mimics one kind of fruit, namely, rambutan.

To compare the current MP-TiO_2-TNW, another two cells based on pure MP-TiO_2 and commercial P25 nanoparticle photoelectrodes were fabricated for comparison (Figure 2j and Table 1). Specifically, the V_{oc} of MP-TiO_2-TNW reduced to 824 mV compared to that of MP-TiO_2 (870 mV) which may be linked to the higher amounts of recombination sites owing to the larger surface area of the high aspect-ratio TiO_2 nanowires coverage. Interestingly, this large surface area causes a dramatic increase of J_{sc} from 8.82 mA cm^{-2} to 16.23 mA cm^{-2}. Consequently, MP-TiO_2-TNW exhibits a nearly 1.7 times higher efficiency of 9.51% as compared to MP-TiO_2 (5.53%). On the other hand, it should be noted that even though MP-TiO_2-TNW and P25 have a similar dye-loading amount (140.7 nmol cm^{-2} vs. 139.5 nmol cm^{-2}), MP-TiO_2-TNW had both a higher V_{oc} (effective recombination suppression) and higher J_{sc} (prominent light-scattering and efficient charge-collection) than P25. As seen in Figure S5, the highest reflectance was found in the 3D MP-TiO_2-TNW, followed by MP-TiO_2 and P25. Given the fact that 3D

Table 1: Summary of device parameters obtained from DSSCs employing various photoanodes with film thickness of approximately 14 μm.

DSSCs	J_{sc} [mA cm^{-2}]	V_{oc} [mV]	η [%]	*FF*	Adsorbed dye/ nmol cm^{-2}
MP-TiO_2	8.82	870	5.53	0.72	60.93
MP-TiO_2-TNW	16.23	824	9.51	0.71	140.7
P25	13.78	803	7.74	0.70	139.5
MP-SnO_2	11.70	751	4.92	0.56	91.0
MP-SnO_2-TNW	15.25	808	7.06	0.57	130.3
MP-Zn_2SnO_4	8.75	753	4.63	0.70	166.4
MP-Zn_2SnO_4-TNW	11.86	783	6.62	0.72	198.9

branched-nanowire-coated macropores with size comparable to the wavelength of the incident light contribute greatly to the strong visible Mie light scattering, the randomly oriented growth of TiO_2 nanowires is also expected to contribute additionally to the improved diffuse scattering. Moreover, the interior cavities induced by interlaced nanowires could function as trapping chambers to confine the incident light and reinforce the light-harvesting by means of multi-reflection. All these factors clearly highlight the superior diffuse scattering of the 3D branched nanowire-coated macroporous structured photoanodes with nanowire scattering centers compared to the pure macropore or nanocrystalline ones, resulting in the significantly improved J_{sc}. Electrochemical impedance spectra (EIS) analysis (Figure 2k) was used to investigate the interfacial recombination of photoexcited electrons within DSSCs, the electron lifetime (τ_r) can be obtained by fitting the EIS spectra according to an equivalent circuit model,[12] and the fitted resistance parameters of R_2 and τ_r are summarized in Table S2. In particular, MP-TiO_2 and MP-TiO_2-TNW show much larger recombination resistance of R_2 and longer electron lifetime of τ_r than the nanoparticle-based films. It indicates the TiO_2 films consisting of hollow spheres play a pivotal role in reducing recombination process. It is generally accepted that slower recombination occurs during the process of charge transfer, the probability of photo-generated electrons being collected becomes higher, which is beneficial to achieve high solar conversion efficiency.

To extend the application of this versatile solution growth of anatase TiO_2 nanowire branches on different macroporous metal oxide scaffolds other than TiO_2 ones, the representative binary oxides (SnO_2) and ternary oxides (Zn_2SnO_4) were selected as the host macroporous scaffolds. Figure 3 presents the SEM images of macroporous SnO_2 (Figure 3a), macroporous Zn_2SnO_4 host (Figure 3d) as well as their corresponding TiO_2 branch modified networks (Figure 3b and e). Accordingly, the TEM images (Figure S6 and Figure S7) clearly show the macroporous coated with nanowires structure of SnO_2–TiO_2 and Zn_2SnO_4–TiO_2 hybrid films. SEM and TEM images reveal the TiO_2 nanowires exhibit different aspect ratios on different metal oxide interfaces. Specifically, 20–60 nm long needle-shaped branches (8–10 nm in diameter) were grown densely and uniformly on the entire inner and outer surface of the macroporous SnO_2 scaffold, which mimics the flower buds of sunflowers (inset in Figure 3b). On the other hand, numerous 100–300 nm long rod-like branches (ca. 20 nm in diameter) preferably encircle the pristine macroporous Zn_2SnO_4 scaffolds to form a nest-like architecture (inset in Figure 3e). The TEM and HRTEM images (Figure S6 and S7) give further insight into the structure of the 3D branched macroporous nanostructures and confirm the anatase crystal structure of TiO_2 nano-branches. The nanowire-coated macroporous material heterostructures, as a proof of concept, were used as photoanodes for DSSCs application and the device performance parameters are summarized in Table 1. The MP-SnO_2-TNW and MP-Zn_2SnO_4-TNW-based devices show significant improvement in both J_{sc} and V_{oc} over that of their pristine macroporous–backbone based devices (Figure 3c and f), resulting in better conversion efficiency of 7.06% for MP-SnO_2-TNW and 6.62% for MP-Zn_2SnO_4-TNW, which are the highest recorded for SnO_2 or Zn_2SnO_4 macroporous or SnO_2–TiO_2, Zn_2SnO_4–TiO_2 heterojunction structured photoelectrode based DSSCs. The enhanced J_{sc} obtained with MP-SnO_2-TNW (from 11.70 mA cm^{-2} to 15.25 mA cm^{-2}) and MP-Zn_2SnO_4-TNW (from 8.75 mA cm^{-2} to 11.81 mA cm^{-2}) can be rationalized in terms of enlarged surface area for boosted dye-loading (Table 1) and better scattering properties (Figure S8) as confirmed by diffused reflectance. Unlike the photovoltage sacrifice behavior which has been observed for homogeneous MP-TiO_2-TNW, an increase of 57 mV and 30 mV for MP-SnO_2-TNW (808 mV) and MP-Zn_2SnO_4-TNW (783 mV) are obtained, respectively, which mainly relate to the conduction band position and recombination dynamics in the cell based on different photoanodes (see below). The EIS, and intensity modulated photocurrent/photovoltage spectra (IMPS/IMVS) results (Figure S9 and Figure S10) indicate that the epitaxial growth of TiO_2 branches on the SnO_2 or Zn_2SnO_4 macroporous scaffold could form a core–shell structure and thus facilitate the transport of photoinduced electrons and suppress the recapture of photoinjected electrons by I_3^- (charge recombination) within DSSCs, leading to increase in photocurrent and photovoltage.[13]

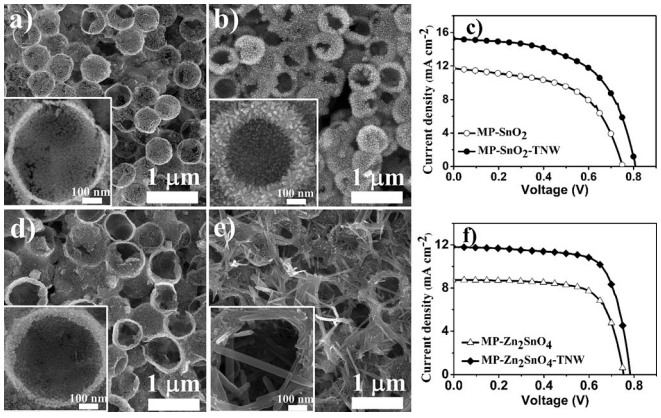

Figure 3. FE-SEM images of a) MP-SnO_2, b) MP-SnO_2-TNW, d) MP-Zn_2SnO_4 and e) MP-Zn_2SnO_4-TNW, respectively; insets are magnified SEM images; c,f) *J*–*V* curves.

The findings of photovoltage improvement motivate further mechanism studies on the role of the interface between the two components (the nanowire and the macroporous material) and the role of the homogeneous or heterogeneous materials at this interface, charge transfer pathways and other electronic properties of the materials with the homo-/heterojunction hybrid structures that could affect photogenerated electron injection dynamics or shift the quasi-Fermi level. We make a comparison for the first time regarding light-intensity dependence of the electron transport time (τ_d) and electron lifetime (τ_r) among MP-TiO_2-TNW, MP-SnO_2-TNW, and MP-Zn_2SnO_4-TNW photoelectrodes based devices with homogeneous or heterogeneous interfaces. Under various light intensities, τ_d increased in the order MP-SnO_2-TNW < MP-TiO_2-TNW < MP-Zn_2SnO_4-TNW and τ_r decreased in the order MP-SnO_2-TNW > MP-Zn_2SnO_4-TNW > MP-TiO_2-TNW (Figure 4a,b). Particular attention

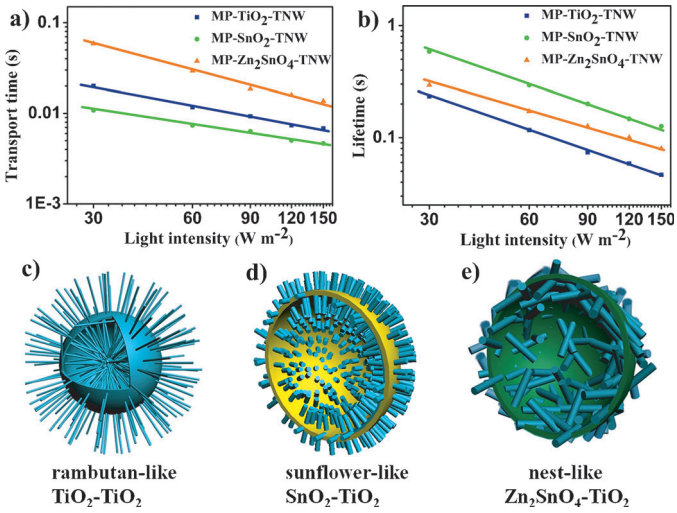

Figure 4. a) Transport time and b) electron lifetime of the DSSCs based on the MP-TiO_2-TNW, MP-SnO_2-TNW and MP-Zn_2SnO_4-TNW photoelectrodes. Schematic diagrams of c) rambutan-like TiO_2–TiO_2, d) sunflower-like SnO_2–TiO_2, and e) nest-like Zn_2SnO_4–TiO_2 are used to illustrate the electrical transfer dynamics.

should be paid on the growth of TiO_2 nanowires with different size distributions and orientation on the surface of various macroporous scaffolds, namely, randomly interlaced TiO_2 nanowires with tiny diameters (3–5 nm) and long lengths (150–200 nm) on homogeneous TiO_2 macroporous scaffolds (rambutan-like MP-TiO_2-TNW, Figure 4c), densely uniform short TiO_2 nanowires with diameter from 8–10 nm and length from 20–60 nm on macroporous SnO_2 scaffold (sunflower-like MP-SnO_2-TNW, Figure 4d), and TiO_2 nanorods of 20 nm in diameter and 100–300 nm in length with a random arrangement on a macroporous Zn_2SnO_4 scaffold (nest-like MP-Zn_2SnO_4-TNW, Figure 4e). Cross-sectional SEM images of these three kinds of photoanodes are in Figure S11. Different sizes of TiO_2 nanowire branches grown on TiO_2, SnO_2, or Zn_2SnO_4 macroporous scaffolds can be probably attributed to the different interfaces between TiO_2–TiO_2, SnO_2–TiO_2 and Zn_2SnO_4–TiO_2 during the homo-/heterogeneous growth. Specifically, it is important to note that MP-SnO_2-TNW based cells allowed the fastest electron transport and slowest charge recombination owing to the short TiO_2 nanowires with uniformly epitaxial orientation on MP-SnO_2 surface providing the most straightforward shortcuts for the injection of photogenerated electrons from TiO_2 to SnO_2 and plus the SnO_2 scaffold allows highest electron mobility (ca. 100 to 200 $cm^2 V^{-1} S^{-1}$)[14] of the three scaffolds. The longest electron lifetime for MP-SnO_2-TNW based cells can be attributed to comparably few electron recombination centers resulting from short TiO_2 nanowires. For the comparison of MP-TiO_2-TNW and MP-Zn_2SnO_4-TNW, although the macroporous Zn_2SnO_4 scaffold offers higher electron mobility (ca. 10 to 15 $cm^2 V^{-1} S^{-1}$) than that of macroporous TiO_2 scaffolds (ca. 0.1 to 10 $cm^2 V^{-1} S^{-1}$),[15] the random arrangement of TiO_2 nanowires on the Zn_2SnO_4 surface build up circuitous pathways for electron transport which hinder the fast electron transportation and thus leading to the slowest electron transport.

The electron lifetime of the MP-TiO_2-TNW based cells comprising the long thin TiO_2 nanowires with interlaced and interconnected network is the shortest of the three systems. In this case, the subsequent growth of TiO_2 branches causes the most significant increase of surface area for dye adsorption by the homogeneous branched TiO_2 macroporous network, which in turn, provides far more recombination centers and surface trapping sites for recombination.

In conclusion, we have synthesized 3D branched-nanowire coated macroporous materials consisting of epitaxial networks of anatase TiO_2 nanowires embedded within various metal oxide scaffolds (for example, TiO_2, SnO_2 and Zn_2SnO_4) through a facile fabrication strategy. Favorable attributes, such as high specific surface area, strong light scattering, and prominent electron transport properties, allows the promise of such novel 3D hierarchical photoanode materials to be demonstrated as suitable concept electrode for enhancing light harvesting, charge collection, and reducing interfacial recombination to significantly increase the photocurrent and photovoltage of DSSCs. Hence, the cells delivered maximum PCE of 9.51%, 7.06%, and 6.62% under full sun illumination for macroporous TiO_2–TiO_2 nanowire, macroporous SnO_2–TiO_2 nanowire and macroporous Zn_2SnO_4–TiO_2 nanowire based hybrid electrodes, respectively. We believe that the simplicity and versatility of these fabrication techniques will open up new opportunities for processing novel materials with 3D geometric architecture that enables structural control on the homogeneous or heterogeneous materials interface, conduction-band position, electron extraction, optical scattering as well as recombination dynamics, to achieve high-efficiency and low-cost solar cells and realize its potential application in the fields such as clean energy, optoelectronics and photocatalysis.

Experimental Section

Hierarchical macroporous metal oxides: The 560 nm polystyrene spheres (PS) were synthesized in an emulsifier-free system.[16] The PS coated by metal oxide nanoparticles (TiO_2, SnO_2, Zn_2SnO_4) was synthesized by a template-assisted method. Concretely, the PS@TiO_2 or PS@SnO_2 was prepared by a refluxing method. PS@TiO_2: butyl titanate (0.4 mL) was mixed with ethanol (20 mL) under vigorous stirring at 70 °C for 12 h followed by addition of an aqueous solution of PS (4 mL) and stirring for another 12 h. PS@SnO_2: typically, a $SnCl_2{\cdot}2H_2O$ ethanol solution (5 mmol; 50 mL) was slowly added to a flask containing distilled H_2O (25 mL) and PS aqueous solution (25 mL) under vigorous stirring and kept in an oil bath at 100 °C for 12 h.[3c] PS@Zn_2SnO_4 enclosed by Zn_2SnO_4 nanoparticles was prepared through a hydrothermal process in accordance with our previous report.[3d] The as-obtained PS@metal oxide solution was then rinsed with ethanol and distilled water, and then uniformly dispersed in ethanol using an ultrasonic bath. Afterwards, the ethanol solution of PS@metal oxide was dripped by a pipet onto a TiO_2 or SnO_2 blocking layer (100 nm thick)-coated FTO glass substrates (7 Ω/square, America) and dried naturally in room temperature. Films with different thickness were controlled by dropping different volumes of the applied dispersions (typically, ca. 100 μL for 10–15 μm thick film). Subsequently, the films were calcined in a box furnace at 500 °C for 1 h to remove PS templates. The resultant TiO_2, SnO_2, and Zn_2SnO_4 films exhibited a hollow sub-microsphere structure with a uniform

distribution and were designated as MP-TiO_2, MP-SnO_2, and MP-Zn_2SnO_4, respectively.

Synthesis of rambutan-like TiO_2–TiO_2, sunflower-like SnO_2–TiO_2 and nest-like Zn_2SnO_4–TiO_2 hybrid electrodes: $K_2TiO(C_2O_4)_2$ (0.35 g) was added to the mixture solvent containing diethylene glycol (DEG) and deionized water in different volume ratios (0:20, 5:15, 10:10, 15:5, 17.5:2.5 and 19:1), whereas the total volume of the solutions was fixed at 20 mL. After stirring for 30 min, the solution was transferred to a 50 mL Teflon-lined stainless steel autoclave. Then as-prepared MP-TiO_2/FTO, MP-SnO_2/FTO and MP-Zn_2SnO_4/FTO films were placed at an angle against the wall of the Teflon-liner with the film side facing down. The hydrothermal synthesis was maintained at 180 °C for 1.5–9 h and was air-cooled to room temperature naturally. Subsequently, the samples were rinsed with deionized water, ethanol, and heated in air at 500 °C for 1 h to increase crystallinity. The MP-TiO_2, MP-SnO_2, and MP-Zn_2SnO_4 covered by TiO_2 nanowires prepared at 180 °C for 6 h were designated as MP-TiO_2-TNW, MP-SnO_2-TNW, and MP-Zn_2SnO_4-TNW, respectively. The assembly of DSSCs[17] and detailed characterizations of the materials and cells can be seen in Supporting Information.

Received: February 14, 2014
Published online: March 26, 2014

Keywords: electron transport · light harvesting · macroporous material · nanowires · solar cells

[1] a) B. O'Regan, M. Grätzel, *Nature* **1991**, *353*, 737 – 740; b) F. Di Fonzo, F. Sauvage, A. L. Bassi, C. S. Casari, V. Russo, G. Divitini, C. Ducati, C. E. Bottani, P. Comte, M. Grätzel, *Nano Lett.* **2010**, *10*, 2562 – 2567; c) Q. F. Zhang, G. Z. Cao, *Nano Today* **2011**, *6*, 91 – 109.

[2] a) S.-H. Han, S. Lee, H. Shin, H. S. Jung, *Adv. Energy Mater.* **2011**, *1*, 546 – 550; b) S. I. Matsushita, N. Fukuda, M. Shimomura, *Colloids Surf. A* **2005**, *257 – 258*, 15 – 17.

[3] a) S. C. Yang, D. J. Yang, J. Kim, J. M. Hong, H. G. Kim, I. D. Kim, H. Lee, *Adv. Mater.* **2008**, *20*, 1059 – 1064; b) J. F. Qian, P. Liu, Y. Xiao, Y. Jiang, Y. L. Cao, X. P. Ai, H. X. Yang, *Adv. Mater.* **2009**, *21*, 3663 – 3667; c) K. N. Li, Y. F. Wang, Y. F. Xu, H. Y. Chen, C. Y. Su, D. B. Kuang, *ACS Appl. Mater. Interfaces* **2013**, *5*, 5105 – 5111; d) Y. F. Wang, K. N. Li, Y. F. Xu, H. S. Rao, C. Y. Su, D. B. Kuang, *Nanoscale* **2013**, *5*, 5940 – 5948; e) Z. H. Dong, X. Y. Lai, J. E. Halpert, N. L. Yang, L. X. Yi, J. Zhai, D. Wang, Z. Y. Tang, L. Jiang, *Adv. Mater.* **2012**, *24*, 1046 – 1049; f) J. Du, J. Qi, D. Wang, Z. Tang, *Energy Environ. Sci.* **2012**, *5*, 6914 – 6918.

[4] a) D. B. Kuang, T. Brezesinski, B. Smarsly, *J. Am. Chem. Soc.* **2004**, *126*, 10534 – 10535; b) W. Fan, M. A. Snyder, S. Kumar, P. S. Lee, W. C. Yoo, A. V. McCormick, R. L. Penn, A. Stein, M. Tsapatsis, *Nat. Mater.* **2008**, *7*, 984 – 991; c) N. Tétreault, E. Arsenault, L. P. Heiniger, N. Soheilnia, J. Brillet, T. Moehl, S. Zakeeruddin, G. A. Ozin, M. Grätzel, *Nano Lett.* **2011**, *11*, 4579 – 4584; d) B. Mandlmeier, J. M. Szeifert, D. Fattakhova-Rohlfing, H. Amenitsch, T. Bein, *J. Am. Chem. Soc.* **2011**, *133*, 17274 – 17282.

[5] a) H. C. Pang, H. B. Yang, C. X. Guo, J. L. Lu, C. M. Li, *Chem. Commun.* **2012**, *48*, 8832 – 8834; b) X. Y. Lai, J. E. Halpert, D. Wang, *Energy Environ. Sci.* **2012**, *5*, 9944 – 9944.

[6] a) M. Law, L. E. Greene, J. C. Johnson, R. Saykally, P. D. Yang, *Nat. Mater.* **2005**, *4*, 455 – 459; b) L. Y. Cao, J. S. White, J. S. Park, J. A. Schuller, B. M. Clemens, M. L. Brongersma, *Nat. Mater.* **2009**, *8*, 643 – 647; c) B. Weintraub, Y. Wei, Z. L. Wang, *Angew. Chem.* **2009**, *121*, 9143 – 9147; *Angew. Chem. Int. Ed.* **2009**, *48*, 8981 – 8985; d) W. Q. Wu, H. S. Rao, Y. F. Xu, Y. F. Wang, C. Y. Su, D. B. Kuang, *Sci. Rep.* **2013**, *3*, 1892; e) Y. G. Wei, C. Xu, S. Xu, C. Li, W. Z. Wu, Z. L. Wang, *Nano Lett.* **2010**, *10*, 2092 – 2096; f) W. Q. Wu, Y. F. Xu, C. Y. Su, D. B. Kuang, *Energy Environ. Sci.* **2014**, *7*, 644 – 649; g) J. Y. Liao, B. X. Lei, H. Y. Chen, D. B. Kuang, C. Y. Su, *Energy Environ. Sci.* **2012**, *5*, 5750 – 5757.

[7] S. K. Karuturi, J. S. Luo, C. W. Cheng, L. J. Liu, L. T. Su, A. I. Y. Tok, H. J. Fan, *Adv. Mater.* **2012**, *24*, 4157 – 4162.

[8] a) A. Kay, M. Grätzel, *Chem. Mater.* **2002**, *14*, 2930 – 2935; b) Y. C. Qiu, W. Chen, S. H. Yang, *Angew. Chem.* **2010**, *122*, 3757 – 3761; *Angew. Chem. Int. Ed.* **2010**, *49*, 3675 – 3679.

[9] a) E. Palomares, J. N. Clifford, S. A. Haque, T. Lutz, J. R. Durrant, *J. Am. Chem. Soc.* **2003**, *125*, 475 – 482; b) S. Ito, P. Liska, P. Comte, R. L. Charvet, P. Pechy, U. Bach, L. Schmidt-Mende, S. M. Zakeeruddin, A. Kay, M. K. Nazeeruddin, M. Grätzel, *Chem. Commun.* **2005**, 4351 – 4353.

[10] a) T. Chen, W. H. Hu, J. L. Song, G. H. Guai, C. M. Li, *Adv. Carbohydr. Anal.* **2012**, *22*, 5245 – 5250; b) C. X. Guo, H. B. Yang, Z. M. Sheng, Z. S. Lu, Q. L. Song, C. M. Li, *Angew. Chem.* **2010**, *122*, 3078 – 3081; *Angew. Chem. Int. Ed.* **2010**, *49*, 3014 – 3017.

[11] W. Q. Wu, B. X. Lei, H. S. Rao, Y. F. Xu, Y. F. Wang, C. Y. Su, D. B. Kuang, *Sci. Rep.* **2013**, *3*, 1352.

[12] J. van de Lagemaat, N. G. Park, A. J. Frank, *J. Phys. Chem. B* **2000**, *104*, 2044 – 2052.

[13] a) H. J. Snaith, C. Ducati, *Nano Lett.* **2010**, *10*, 1259 – 1265; b) A. B. F. Martinson, J. W. Elam, J. Liu, M. J. Pellin, T. J. Marks, J. T. Hupp, *Nano Lett.* **2008**, *8*, 2862 – 2866.

[14] I. Abayev, A. Zaban, F. Fabregat-Santiago, *J. Phys. Status Solidi A* **2003**, *196*, R4 – R6.

[15] T. J. Coutts, D. L. Young, X. Li, W. P. Mulligan, X. Wu, *J. Vac. Sci. Technol. A* **2000**, *18*, 2646 – 2660.

[16] J. W. Goodwin, J. Hearn, C. C. Ho, R. H. Ottewill, *Colloid Polym. Sci.* **1974**, *252*, 464 – 471.

[17] W. Q. Wu, Y. F. Xu, H. S. Rao, C. Y. Su, D. B. Kuang, *Nanoscale* **2013**, *5*, 4362 – 4369.

